

A thermodynamic model for estimating sea and lake ice thickness with optical satellite data

Xuanji Wang,¹ Jeffrey R. Key,² and Yinghui Liu¹

Received 30 September 2009; revised 4 August 2010; accepted 13 September 2010; published 16 December 2010.

[1] Sea ice is a very important indicator and an effective modulator of regional and global climate change. Current remote sensing techniques provide an unprecedented opportunity to monitor the cryosphere routinely with relatively high spatial and temporal resolutions. In this paper, we introduce a thermodynamic model to estimate sea and lake ice thickness with optical (visible, near-infrared, and infrared) satellite data. Comparisons of nighttime ice thickness retrievals to ice thickness measurements from upward looking submarine sonar show that this thermodynamic model is capable of retrieving ice thickness up to 2.8 m. The mean absolute error is 0.18 m for samples with a mean ice thickness of 1.62 m, i.e., an 11% mean absolute error. Comparisons with in situ Canadian stations and moored upward looking sonar measurements show similar results. Sensitivity studies indicate that the largest errors come from uncertainties in surface albedo and downward solar radiation flux estimates from satellite data, followed by uncertainties in snow depth and cloud fractional coverage. Due to the relatively large uncertainties in current satellite retrievals of surface albedo and surface downward shortwave radiation flux, the current model is not recommended for use with daytime data. For nighttime data, the model is capable of resolving regional and seasonal variations in ice thickness and is useful for climatological analysis.

Citation: Wang, X., J. R. Key, and Y. Liu (2010), A thermodynamic model for estimating sea and lake ice thickness with optical satellite data, *J. Geophys. Res.*, 115, C12035, doi:10.1029/2009JC005857.

1. Introduction

[2] Changes in sea ice significantly affect the exchanges of momentum, heat, and mass between the sea and the atmosphere. While sea ice extent is an important indicator and effective modulator of regional and global climate change, sea ice thickness is the more important parameter from a thermodynamic perspective.

[3] There are some ice thickness data from submarine Upward-Looking Sonar (ULS) during various field campaigns, for instance, the Scientific Ice Expeditions (SCICEX) in 1996, 1997, and 1999 [*National Snow and Ice Data Center*, 2006]. There are some in situ measurements of ice thickness from the New Arctic Program initiated by the Canadian Ice Service (CIS) starting in 2002, and sea ice draft measurements from moored ULS instruments in the Beaufort Gyre Observing System (BGOS). There are a few studies on changes in sea ice thickness and volume, but they are for specific locations over a limited time period, such as the work by *Rothrock et al.* [2008] using the ice draft profiles from submarine transects. The amount of available ice thickness data is insufficient for most large-scale studies.

[4] Many numerical ocean-sea ice-atmosphere models can, to large extent, simulate sea ice extent with sufficient accuracy to capture its spatial and temporal distributions, as demonstrated by the Intergovernmental Panel on Climate Change Fourth Assessment Report (IPCC AR4) models [*Zhang and Walsh*, 2006]. Only a few numerical ocean-sea ice-atmosphere models simulate ice thickness distribution, notably, the Pan-Arctic Ice-Ocean Modeling and Assimilation System (PIOMAS) developed by *Zhang and Rothrock* [2003]. All the model simulations have relatively low spatial resolution compared to satellite data.

[5] Accurate, consistent ice thickness data with high spatial resolution are critical for a wide range of applications including climate change detection, climate modeling, and operational applications such as shipping and hazard mitigation. Satellite data provide an unprecedented opportunity to monitor the cryosphere routinely with relatively high spatial and temporal resolutions for both sea ice, and lake and river ice.

[6] Spaceborne sensors, particularly passive microwave radiometers and synthetic aperture radar, have been used primarily to map ice extent and ice concentration, and to monitor and study their trends [*Comiso*, 2002; *Francis et al.*, 2009; *Francis and Hunter*, 2007; *Maslanik et al.*, 2007; *Drobot et al.*, 2008]. Some sea ice thickness data have been estimated from satellite radar altimetry since 1993 [*Laxon et al.*, 2003], and will be estimated in the future from the recently launched European Space Agency (ESA) CryoSat-2

¹Cooperative Institute of Meteorological Satellite Studies, University of Wisconsin-Madison, Madison, Wisconsin, USA.

²NESDIS, NOAA, Madison, Wisconsin, USA.

mission (http://www.esa.int/esaLP/ESAOMH1VMOC_LPcryosat_0.html). With the launch of the ICESat satellite in January of 2003, sea ice thickness and volume estimation methods were developed for use with elevation data from ICESat's laser altimeter [Kwok and Cunningham, 2008; Kwok et al., 2009; Zwally et al., 2008].

[7] Can the longer-term records of optical (visible, near-infrared, infrared) satellite data onboard polar orbiting satellites be used to retrieve ice thickness? Since the first launch of the U.S. National Oceanic and Atmospheric Administration (NOAA) Television and InfraRed Observation Satellite (TIROS) series in 1962, the Advanced Very High Resolution Radiometer (AVHRR) has been widely used in many geophysical applications including the mapping of ice extent. Can optical satellite imagers such as the AVHRR and Moderate Resolution Imaging Spectroradiometer (MODIS) also be used to estimate ice thickness? Some work has been done in this field [cf. Yu and Rothrock, 1996]. However, those studies have been limited to case studies of thin ice.

[8] This paper presents a model based on ice surface energy budget to estimate sea and lake ice thickness with optical satellite data. This model is capable of deriving ice thickness up to 2.8 m under both clear- and cloudy-sky conditions with accuracy of greater than 80%. This paper is organized as follows. Section 2 describes the physics of the model with its three components: radiative, turbulent, and conductive fluxes. Applications of the model using different satellite data for ice thickness retrievals are given in section 3. Section 4 presents validation results of ice thickness retrievals using this model with submarine, station, and mooring data in the Arctic. Quantitative analysis of the uncertainties and sensitivities of our model is discussed in section 5. Discussion and conclusions follow in section 6.

2. One-Dimensional Thermodynamic Ice Model

[9] A slab model proposed by Maykut and Untersteiner [1971] is used here as the basis for our One-dimensional Thermodynamic Ice Model (OTIM). The general equation for energy conservation at the surface (ice or snow) is

$$(1 - \alpha_s)F_r - I_0 - F_l^{up} + F_l^{dn} + F_s + F_e + F_c = F_a \quad (1)$$

where α_s is the ice or snow covered surface shortwave broadband albedo, F_r is the downward shortwave radiation flux at the surface, I_0 is the shortwave radiation flux passing through the ice interior with ice slab transmittance i_0 , F_l^{up} is the upward longwave radiation flux from the surface, F_l^{dn} is the surface downward longwave radiation flux from the atmosphere, F_s is the sensible heat flux at the surface, F_e is the latent heat flux at the surface, F_c is the conductive heat flux within the ice slab, and F_a is the residual heat flux that could be caused by ice melting and/or heat horizontal advection. Flux entering the surface is positive, and flux leaving the surface is negative. By definition, in equation (1), α_s , F_r , I_0 , F_l^{up} , F_l^{dn} should be always positive, F_s , F_e , and F_c could be positive or negative, and F_a is usually assumed to be zero in the absence of a phase change. The details of each term will be addressed in sections 2.1 through 2.7.

2.1. Shortwave Radiation at the Surface and Through the Ice

[10] The first term on the left-hand side of equation (1), $(1 - \alpha_s)F_r$, is the net shortwave radiation flux at the surface. The surface broadband albedo over entire solar spectrum, α_s , is estimated [Grenfell, 1979] by

$$\alpha_s = 1 - A \exp(-Bh) - C \exp(-Dh) \quad (2)$$

where A , B , C , and D are empirically derived coefficients, and h is the ice thickness (h_i) or snow depth (h_s) in meter if snow is present over the ice. The other relatively simple approaches to determine ice and snow surface albedo include model simulated constant values based on the ice and snow types as discussed by Saloranta [2000], and the experimental and observational values for a variety of snow and ice surface conditions as discussed by Grenfell and Perovich [2004]. Equation (2) is chosen for surface albedo estimation is based on the following considerations. (1) It is not constant but a function of ice thickness, ice type, and snow depth. (2) The coefficients A , B , C , and D are dependent on ice types and snow depth, and different for clear- and cloudy-sky conditions that make it suitable for use with satellite data. (3) It is relatively easy to improve the broadband albedo estimation by adjusting A , B , C , and D values accordingly with more updated validation results. The values of A , B , C , and D are given by Grenfell [1979, Table 1]. The downward shortwave radiation flux at the surface, F_r , can be either an input parameter or parameterized with parameterization schemes built into the OTIM. There are a number of parameterization schemes estimating F_r under both clear- and cloudy-sky conditions for cold regions. Key et al. [1996] compared these schemes for applications in high latitude, including clear-sky parameterization schemes from Shine and Henderson-Sellers [1985], Moritz [1978], and Bennett [1982], and cloudy-sky parameterization schemes from Shine [1984], Bennett [1982], Jacobs [1978], Laevastu [1960], and Berliand [1960]. For clear- and cloudy-sky downward shortwave radiation fluxes in the OTIM, the Shine [1984] schemes are used.

[11] The second term on the left-hand side of equation (1), $I_0 = i_0(1 - \alpha_s)F_r$, is the shortwave radiation flux passing through the ice interior. i_0 is the ice slab transmittance, i.e., the percentage of the shortwave radiation flux that penetrates the ice, which is estimated by the following parameterization scheme by Grenfell [1979]:

$$i_0 = A \exp(-Bh) + C \exp(-Dh) \quad (3)$$

where A , B , C , and D are coefficients that are different from those in equation (2), and h is the ice slab thickness in meters.

2.2. Longwave Radiation at the Surface

[12] The third term on the left-hand side of equation (1), F_l^{up} , is the upward longwave radiation flux from the surface to the atmosphere, which is estimated with

$$F_l^{up} = \varepsilon \sigma T_s^4 \quad (4)$$

where ε is the longwave emissivity of the ice or snow surface, σ is the Stefan-Boltzman constant, and T_s is the surface

skin temperature in K. For simplicity, an ice emissivity of 0.988 is used. Even though some pixels contain a small portion of open water or snow, the error in emissivity from improperly defining the surface type is small because snow emissivity at a 0 degree look angle is 0.995, very close to the value of 0.987 for ice and 0.988 for water [Rees, 1993].

[13] The fourth term on the left-hand side of equation (1), F_l^{dn} , is the surface downward longwave radiation flux from the atmosphere. There are five potential clear-sky parameterization schemes for estimating the downward longwave radiation flux: *Yu and Rothrock* [1996], *Efimova* [1961], *Ohmura* [1981], *Maykut and Church* [1973], and *Andreas and Ackley* [1982]. There are also five potential cloudy-sky parameterization schemes: *Yu and Rothrock* [1996], *Jacobs* [1978], *Maykut and Church* [1973], *Zillman* [1972], and *Schmetz and Raschke* [1986]. Based on the *Key et al.* [1996] study, the *Efimova* [1961] scheme is the most accurate for clear-sky conditions: $F_{l,clr}^{dn} = \sigma T_a^4 (0.746 + 0.0066 e_a)$, where e_a is the water vapor pressure (hPa) near the surface, and T_a is the air temperature at 2 m above the surface. For cloudy-sky conditions, the *Jacobs* [1978] scheme is the best estimator: $F_l^{dn} = F_{l,clr}^{dn} (1 + 0.26C)$, where C is fractional cloud cover. These two schemes are used for estimating the downward longwave radiation flux at the surface.

2.3. Surface Sensible Heat Flux

[14] The fifth term on the left-hand side of equation (1), F_s , is the surface sensible heat flux, which is calculated by following formula:

$$F_s = \rho_a C_p C_s u (T_a - T_s) \quad (5)$$

where ρ_a is the air density (standard value of 1.275 kg m^{-3} at 0°C and 1000 hPa), C_p is the specific heat of wet air with wet air specific humidity q , C_s is the bulk transfer coefficient for sensible heat flux between the air and ice surface (*Yu and Rothrock* [1996] use $C_s = 0.003$ for very thin ice, and 0.00175 for thick ice, 0.0023 for neutral stratification as suggested by *Lindsay* [1998] in his energy balance model for thick Arctic pack ice), u is the surface wind speed, T_a is the near surface air temperature at 2 m above the ground, and T_s is the surface skin temperature. The wet air density ρ_a is calculated using the gas law with surface air pressure P_a in hPa, surface air virtual temperature T_v in K, and the gas constant R_{gas} ($287.1 \text{ J kg}^{-1} \text{ K}^{-1}$) by the formula $\rho_a = \frac{100P_a}{R_{gas}T_v}$, where $T_v = (1 + 0.608q)T_a$ and q is the wet air specific humidity (kg/kg). The wet air specific heat is

$$C_p = C_{pd} \left(1 - q + \frac{C_{pv}}{C_{pd}} q \right) \quad (6)$$

where C_{pv} is the specific heat of water vapor at constant pressure ($1952 \text{ J K}^{-1} \text{ kg}^{-1}$) and C_{pd} is the specific heat of dry air at constant pressure ($1004.5 \text{ J K}^{-1} \text{ kg}^{-1}$), so C_p can simply be written as $C_p = 1004.5 \cdot (1 + 0.9433q)$. The relative humidity over the snow/ice is assumed to be 90%, if it is unknown.

2.4. Surface Latent Heat Flux

[15] The sixth term on the left-hand side of equation (1), F_e , is the latent heat flux at the surface. It is calculated in the OTIM with

$$F_e = \rho_a L C_e u (w_a - w_{sa}) \quad (7)$$

where ρ_a is the air density, L is the latent heat of vaporization ($2.5 \times 10^6 \text{ J kg}^{-1}$) which should include the latent heat fusion/melting ($3.34 \times 10^5 \text{ J kg}^{-1}$) if the surface is below freezing, C_e is the bulk transfer coefficient for latent heat flux of evaporation, u is the surface wind speed, w_a is the air mixing ratio at 2 m above the ground, and w_{sa} is the mixing ratio at the surface. The mixing ratio is very close to the specific humidity in magnitude, $w = q/(1 - q) \cong q$.

[16] The bulk transfer coefficient, C_e , for the latent heat flux is a function of wind speed and/or air-sea ice temperature difference. It can be parameterized as described by *Bentamy et al.* [2003] and used in this study by the formula $C_e = \{a \exp[b(u + c)] + d/u + 1\} \times 10^{-3}$, where $a = -0.146785$, $b = -0.292400$, $c = -2.206648$, and $d = 1.6112292$. The C_e value ranges between 0.0015 and 0.0011 for wind speeds between 2 and 20 m s^{-1} . Another parameterization scheme of C_e was developed by *Kara et al.* [2000] for use in a general circulation model. They related C_e to both surface wind speed and air-sea ice temperature difference:

$$C_e = C_{e0} + C_{e1}(T_s - T_a)$$

$$C_{e0} = [0.994 + 0.061\hat{u} - 0.001\hat{u}^2] \times 10^{-3}$$

$$C_{e1} = [-0.020 + 0.691(1/\hat{u}) - 0.871(1/\hat{u})^2] \times 10^{-3}$$

where the wind speed is limited to the interval $\hat{u} = \max[3.0, \min(27.5, u)]$ to suppress the underestimation of the quadratic fit when $u > 27.5 \text{ m s}^{-1}$.

[17] Because C_s is so close in value to C_e , a linear relationship between C_e and C_s is used rather than determining C_s independently. The simplest representative linear formulation is found to be $C_s = 0.96C_e$ with a negligible intercept (3.6×10^{-6}) as reported by *Kara et al.* [2000]; we use $C_s = 0.98C_e$ in our model for air-sea ice interface turbulent heat transfer.

2.5. Conductive Heat Flux

[18] The seventh term on the left-hand side of equation (1), F_c , is the conductive heat flux for a two-layer system with one snow layer over an ice slab that can be written as

$$F_c = \gamma(T_f - T_s) \quad (8)$$

where $\gamma = (k_i k_s)/(k_s h_i + k_i h_s)$, T_f is the water freezing temperature (degrees C) that can be derived from the simplified relationship $T_f = -0.055S_w$, where S_w is the salinity of seawater, assumed to be 31.0 parts per thousand (ppt) for the Beaufort Sea and 32.5 ppt for the Greenland Sea, h_s is the snow depth, and h_i is the ice thickness. k_s is the conductivity of snow which can be formulated by $k_s = 2.845 \times 10^{-6} \rho_{\text{snow}}^2 + 2.7 \times 10^{-4} \cdot 2.0^{(T_{\text{snow}} - 233)/5}$ [Ebert and Curry, 1993] that is used in this study, ρ_{snow} is the snow density ranging from 225 kg m^{-3} (new snow) to 450 kg m^{-3} (water-soaked snow), T_{snow} is the snow temperature in K. k_s can be further sim-

plified as $k_s = 2.22362 \times 10^{-5.655} (\rho_{\text{snow}})^{1.885}$ [Yen, 1981]. k_i is the conductivity of ice that is estimated by $k_i = k_0 + \beta S_i / (T_i - 273)$ [Untersteiner, 1964] that is adopted in this study, where $\beta = 0.13 \text{ W m}^{-2} \text{ kg}^{-1}$, $k_0 = 2.22(1 - 0.00159T_i) \text{ W m}^{-1} \text{ K}^{-1}$ that is the conductivity of pure ice [Curry and Webster, 1999]. S_i is the sea ice salinity and T_i is the temperature within the ice slab. Some experimental relationships between h_s and h_i , T_i and T_s , S_i and h_i exist, as described in sections 2.6 and 2.7.

[19] It should point out that assuming linear vertical temperature profile in the ice slab, which means that conductive heat flux across the ice slab is uniform, may cause error in the ice thickness estimation. According to the Zhang and Rothrock's [2001] simulations, the difference in the annual mean ice thickness of 2.52 m between the three-layer model with nonlinear vertical temperature profile and the zero-layer model with linear vertical temperature profile is 0.07 m, or 3%. Based on their simulations, it is reasonable to assume a linear vertical temperature profile in the ice slab, i.e., conductive heat flux across the ice slab is uniform, in our model for dealing with ice thickness less than 3 m.

2.6. Relationships Between Snow Depth and Ice Thickness, Surface Temperature and Ice Temperature, and Sea Ice Thickness and Sea Ice Salinity

[20] Doronin [1971] used the following relationship to estimate snow depth as a function of ice thickness, which was also used by Yu and Rothrock [1996]:

$$h_s = 0 \text{ for } h_i < 5 \text{ cm,}$$

$$h_s = 0.05h_i \text{ for } 5 \text{ cm} \leq h_i \leq 20 \text{ cm,}$$

$$h_s = 0.1h_i \text{ for } h_i > 20 \text{ cm.}$$

In the real world, snow accumulation over the ice may not follow the simple relationship above. So if snow depth is available, it should be input to the model.

[21] The ice temperature T_i is an important factor in the ice conductivity calculation. It may be significantly different from surface skin temperature that can be measured or retrieved with remote sensed data when there is snow on the ice. In general, we can obtain the surface skin temperature T_s from satellite with optical data, but not T_i . Yu and Rothrock [1996] suggested that assuming T_i equal to T_s can cause 5% and 1% errors, when ice thickness is 5 cm and 100 cm, respectively. The assumption that the two are equal may be more valid during the night than the daytime when the surface heating from the Sun increases the difference between the skin (snow) and ice temperatures. Uncertainty in T_i is one source of errors for the daytime retrieval of ice thickness with the OTIM. However, the sensitivity study described later shows that the error in T_i has a smaller effect on the ice thickness derivation than other uncertainties as like from snow depth and cloud fraction.

[22] There are at least three schemes for the relationship between sea ice thickness h_i and sea ice salinity S_i . The Cox and Weeks [1974] scheme is

$$S_i = 14.24 + 19.39h_i \text{ for } h_i \leq 0.4 \text{ m,}$$

$$S_i = 7.88 + 1.59h_i \text{ for } h_i > 0.4 \text{ m.}$$

Jin et al. [1994] gave this relationship:

$$S_i = 7.0 - 31.63h_i \text{ for } h_i \leq 0.3 \text{ m,}$$

$$S_i = 8.0 - 1.63h_i \text{ for } h_i > 0.3 \text{ m.}$$

Kovacs [1996] used this scheme:

$$S_i = 4.606 + 0.91603/h_i \text{ for } 0.10 \text{ m} \leq h_i \leq 2.0 \text{ m.}$$

In the OTIM, we use Kovacs' scheme to express the relationship between sea ice thickness and sea ice salinity.

2.7. Surface Air Temperature

[23] Surface air temperature T_a at 2 m height above the ground is an essential parameter for the OTIM to estimate the surface downward longwave radiation, sensible, and latent heat fluxes. Numerical model forecasts generally do not provide good estimates of the surface 2 m air temperature in the polar regions. Thus, if we assume that large-scale heat sources and sinks, e.g., "hot" leads and cold ice floes, regulate the cold surface 2 m air temperature T_a , therefore T_a should be close to the surface skin temperature T_s overall. Here we assume that

$$T_a = T_s + \delta T \quad (9)$$

where T_s is the surface skin temperature from satellite retrievals, and δT is a function of cloud amount. δT is about 2.2°C for clear-sky conditions, and reduces to about 0.4°C for overcast sky condition as implied by Persson et al. [2002]. Here we set $\delta T = 2.2 - 1.8C_f$ where C_f is the cloud amount ranging from 0 to 1.

3. OTIM Applications With Satellite Data

[24] This section describes the applications of the OTIM with satellite data to estimate ice thickness. While any optical satellite data can be used, the applications with data from NOAA's AVHRR and NASA's MODIS are detailed. Case studies using data from the Spinning Enhanced Visible and InfraRed Imager (SEVIRI) on the Meteosat Second Generation (MSG) satellite, and from the Geostationary Operational Environmental Satellite (GOES) have also been performed, though the results are not presented here. Regardless of the data source, satellite products required by OTIM as inputs are cloud amount, surface skin temperature, surface broadband albedo, and surface downward shortwave radiation fluxes. The latter two are for daytime retrieval only.

[25] The AVHRR Polar Pathfinder extended (APP-x) product suite used in this study [Wang and Key, 2003, 2005; Wang et al., 2007; Fowler et al., 2007] can be found with its product description at <http://stratus.ssec.wisc.edu/projects/app/app.html>. Figure 1 gives an example of the OTIM retrieved sea ice thickness from APP-x data set on 21 February 2004 at 04:00am local solar time. For MODIS data, MODIS cloud mask [Ackerman et al., 1998; Liu et al., 2004] and surface skin temperature are used as inputs to the OTIM. The MODIS and AVHRR ice surface skin temperature for clear-sky conditions is retrieved using a split-

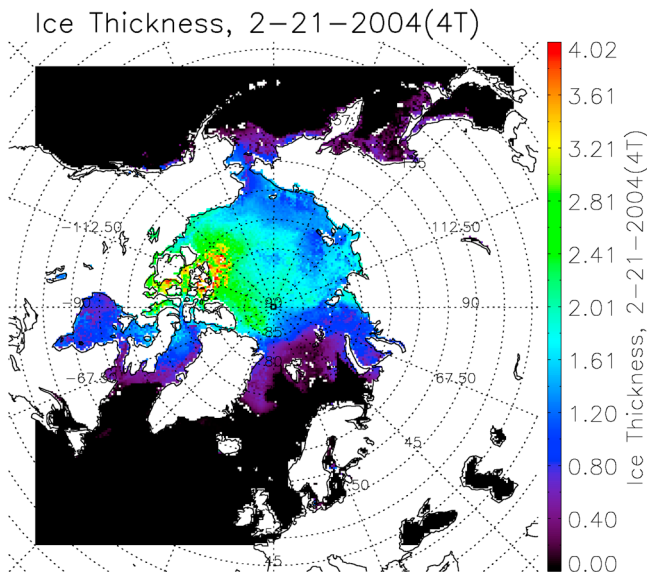


Figure 1. OTIM retrieved sea ice thickness (m) from APP-x data set on 21 February 2004 at 0400 local solar time under all-sky conditions.

window technique, where split window refers to brightness temperature in the 11–12 μm atmospheric window. The retrieval equation is

$$T_s = a + bT_{11} + c(T_{11} - T_{12}) + d[(T_{11} - T_{12})(\sec \theta - 1)] \quad (10)$$

where T_s is the estimated surface temperature (K), T_{11} and T_{12} are the brightness temperatures (K) at 11 μm (MODIS band 31, AVHRR band 4) and 12 μm (MODIS band 32, AVHRR band 5) bands, and θ is the sensor scan angle. More details about this algorithm are given by Key [2002], Key *et al.* [1997a], and Hall *et al.* [2004]. An example of MODIS data application with the OTIM is given in Figure 2.

4. OTIM Validation

[26] To evaluate the performance and accuracy of the OTIM, we validate the ice thickness retrievals using OTIM with ice thickness from submarine cruises, meteorological stations, mooring sites, and numerical model simulations. The APP-x data together with sea ice concentration from Nimbus-7 SMMR and DMSP SSM/I Passive Microwave Data available at <http://nsidc.org/data/nsidc-0051.html> [Cavalieri *et al.*, 2008] were used in the calculation of sea ice thickness with OTIM. The pixel-level sea ice concentration was used to correct sea ice temperature by removing open water temperature contribution from overall ice covered pixel temperature.

4.1. Comparison With Submarine Sonar Measurements

[27] The National Snow and Ice Data Center (NSIDC) archives submarine Upward Looking Sonar (ULS) ice draft (the thickness of the ice below the water line) profile data collected by both U.S. Navy and U.K. Royal Navy submarines in the Arctic Ocean. U.S. Navy guidance has stated that previously classified, submarine-collected ice draft data

may be declassified and released according to set guidelines. Those guidelines include restrictions that positions of the data must be rounded to the nearest 5 min of latitude and longitude, and the date rounded to the nearest third of a month. Due to the limitations enforced by those guidelines, almost all the data are not suitable for ice thickness validation due to the lack of accuracy in the submarine locations.

[28] The Scientific Ice Expeditions (SCICEX) used U.S. Navy submarines for research. SCICEX data are not classified, and thus has precise location and date for all the observations. In this work, we use all SCICEX 1996, 1997, and 1999 ice draft data (hereinafter SCICEX 96, SCICEX 97, and SCICEX 99) taken along the submarine trajectories as shown in Figure 3 because NSIDC obtained permission to release them, which covers 13 September to 28 October for SCICEX 96 data, 3 September to 2 October for SCICEX 97 data, and 3 April to 11 May for SCICEX 99 data. All SCICEX data have two types of files, ice draft profiles and derived statistics. Each ice draft file includes a header that gives the date and two end points for the profile, followed by a sequential list of ice drafts spaced at 1.0 m intervals that comprise the bottomside sea-ice roughness profile. Data in each file fall along a straight-line (great circle) track between the two end points. The length of the profile in any given file can be up to 50 km, but may be shorter if data dropouts create gaps greater than 0.25 km, or if changes in course cause deviations from a straight-line track. Submarine ice draft data were converted to ice thickness with a multiplicative factor of 1.11, based on Archimedes' buoyancy principle. Each derived statistics file includes information on ice draft characteristics such as keels, level ice, leads, undeformed, and deformed ice (refer to <http://nsidc.org/data/g01360.html>).

[29] For each submarine track, ice thickness simulated using the PIOMAS model [Zhang and Rothrock, 2003], with grid size 25 km, was obtained. We are able to compare ice thickness retrievals using OTIM with ice thickness

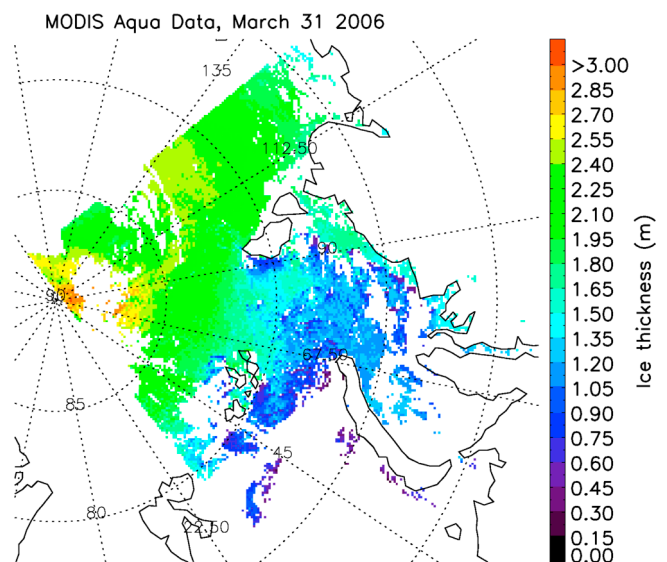


Figure 2. OTIM retrieved Arctic sea ice thickness from MODIS Aqua data on 31 March 2006 under clear-sky conditions.

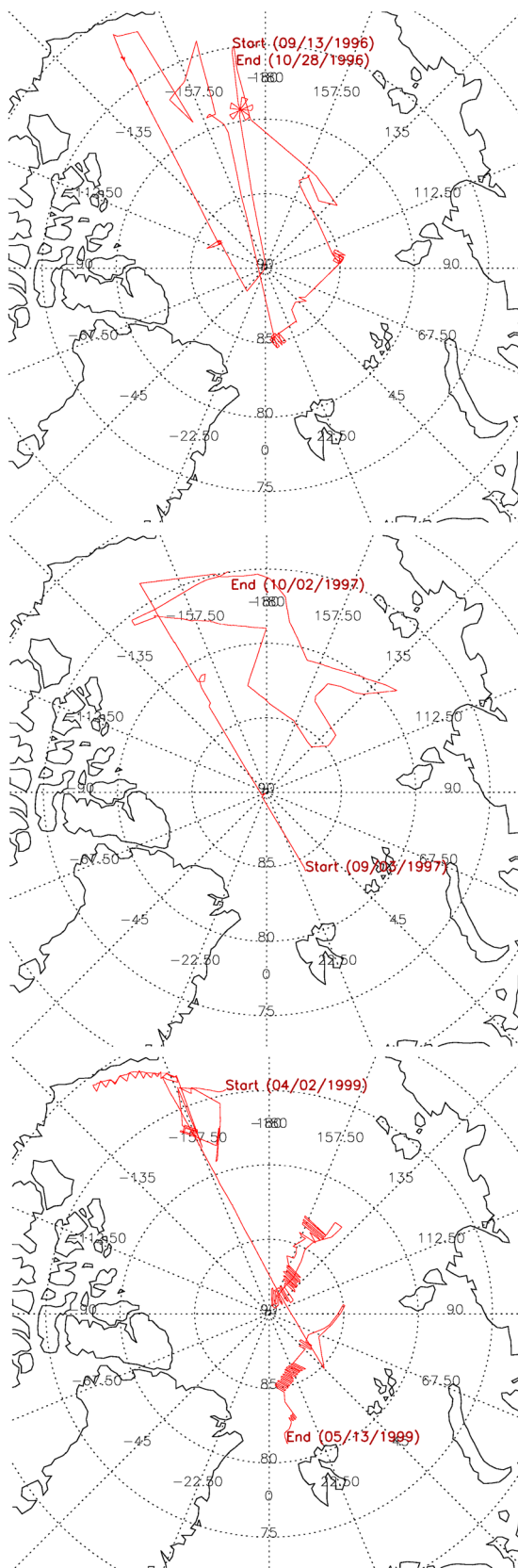


Figure 3. Submarine trajectories for (top) SCICEX 96, (middle) 97, and (bottom) 99. Data with their starting and ending places and dates are marked.

measured by submarines and the corresponding numerical model simulations using PIOMAS. Only those submarine track segments longer than 25 km are used in this comparison because the satellite product and numerical model grid resolutions are 25 km. For each of the locations of submarine track segments, mooring sites, and meteorological stations, the nearest valid pixel within a 3 by 3 pixel box centered at the location from satellite and numerical model data grids on the same date is used for the comparison. If no valid pixel is found within that box from any one of the data sources, in particular, from satellite data grid, the comparison will not be done for that date at the location.

[30] Figure 4 shows comparisons in cumulative frequency of sea ice thickness that were retrieved by OTIM with APP-x data, measured by submarines, and simulated by PIOMAS model. Figure 5 shows the point-to-point comparisons among them. Table 1 lists the comparison results between OTIM and submarine measurements. The overall mean ice thicknesses are 1.62 m and 1.64 m from all SCICEX data and OTIM retrievals, respectively.

[31] The overall mean absolute bias (mean of the absolute values of the differences) between the OTIM and submarine data is 0.18 m, or less than 12% error in terms of true mean ice thickness. The errors are 16% and 10% for 0.00–1.80 m thick ice and 1.80–3.00 m thick ice, respectively. Many factors contribute to the ice thickness differences between the OTIM and submarine data: (1) The actual length of the submarine track segments, and the minimum and maximum ice draft values from the statistics of the submarine track segments. (2) Incorrect cloud identification with satellite data is one of the error sources of OTIM retrievals along with other uncertainties in the retrievals of surface physical parameters, e.g., surface temperature. (3) The submarines made measurements along a line with a particular orientation, while the OTIM retrieved ice thickness is an area average. (4) The designated snow depth of 0.20 m is not applicable to all submarine track segments.

4.2. Comparison With Canadian Meteorological Station Measurements

[32] The Canadian Ice Service (CIS) maintains archived ice thickness and on-ice snow depth measurements for Canadian stations back as far as 1947 for the first established stations in the Canadian Arctic (Eureka and Resolute). By the beginning of 2002 most stations from the original ice thickness program had stopped taking measurements. Fortunately, due to an increasing interest in updating this historical data set to support climate change studies, a new program was started in the fall of 2002, called New Arctic Program (refer to <http://ice-glaces.ec.gc.ca/App/WsvPageDsp.cfm?Lang=eng&lnid=5&ScndLvl=no&ID=11703>). The stations in this program are listed in Table 2, and their data are used here for OTIM validation.

[33] Most of the data in the current archive at the CIS have been collected by the Atmospheric Environment Program of Environment Canada, and some data are provided by other organizations such as the St Lawrence Seaway Authority, Trent University, and Queen's University. Measurements are taken at approximately the same location every year on a weekly basis starting after freeze up when the ice is safe to walk on, and continuing until breakup or when the ice becomes unsafe. Therefore, the measured ice thickness mini-

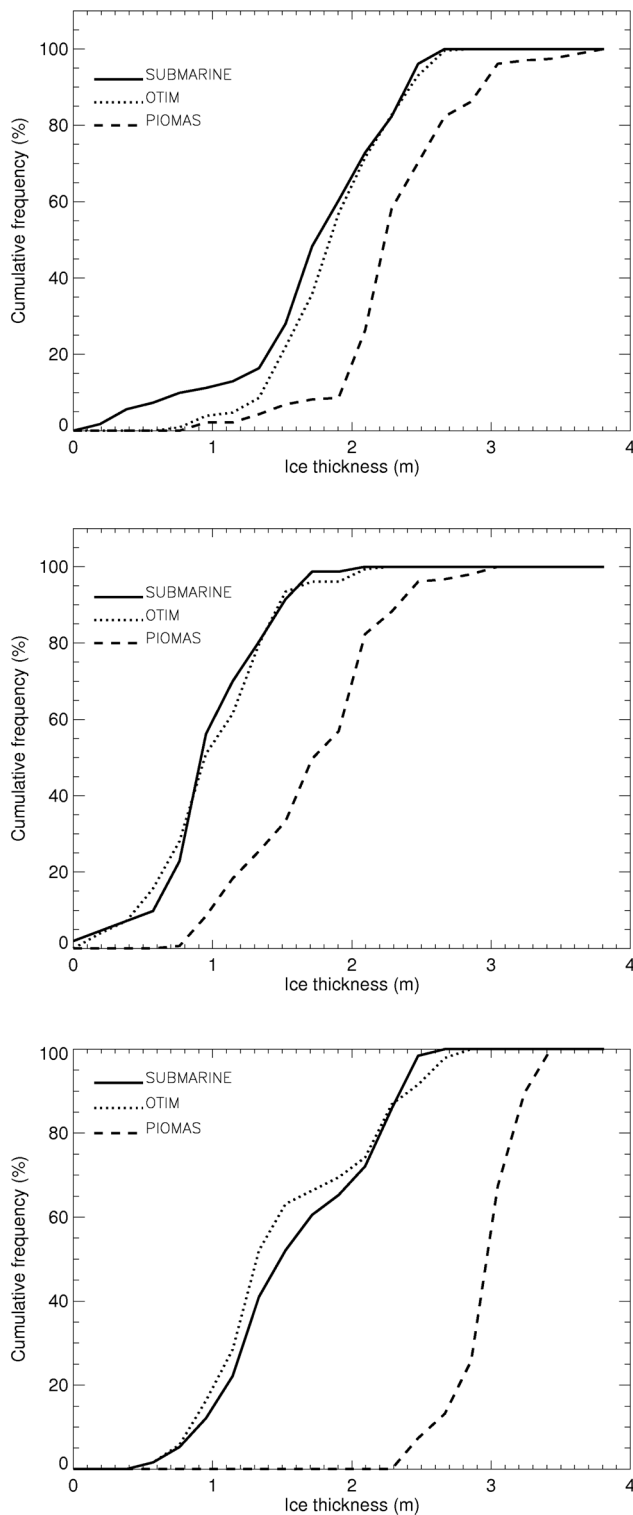


Figure 4. Comparisons of the ice thickness cumulative distribution retrieved by OTIM with APP-x data, simulated by PIOMAS model, and calculated from (top) SCICEX 96, (middle) SCICEX 97, and (bottom) SCICEX 99 data. Submarine ice draft (mean and median only) was converted to ice thickness by a factor of 1.11.

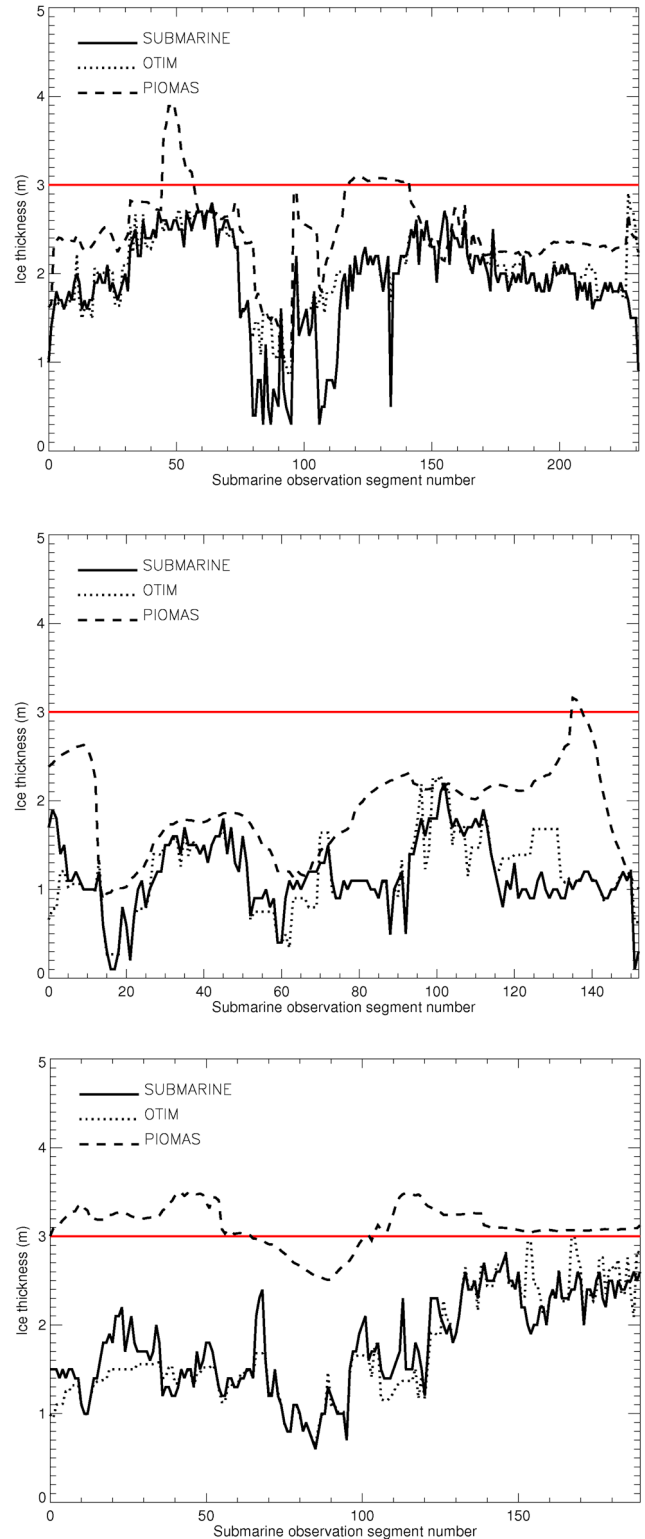


Figure 5. Comparisons of ice thickness values retrieved by OTIM with APP-x data, simulated by PIOMAS model, and calculated from (top) SCICEX 96, (middle) SCICEX 97, and (bottom) SCICEX 99 data along the submarine track segments. Submarine ice draft (mean and median only) was converted to ice thickness by a factor of 1.11.

Table 1. OTIM Retrieved Ice Thickness Validation Results Against SCICEX 96, 97, and 99 Data^a

SCICEX Data OTIM	Thickness Mean (m)	Bias Mean (m)	Bias Absolute Mean (m)
SCICEX 96	1.90	0.13 (6.8%)	0.19 (10.0%)
OTIM	2.03		
SCICEX 97	1.17	0.01 (0.9%)	0.17 (14.5%)
OTIM	1.18		
SCICEX 99	1.78	-0.06 (-3.4%)	0.17 (9.6%)
OTIM	1.72		
All SCICEX Data	1.62	0.02 (1.2%)	0.18 (11.1%)
OTIM average	1.64		

^aThe percentage number in parentheses is the percent error in terms of true mean ice thickness.

imum is 20 cm for almost all of the stations. The location of the ice thickness measurement is selected close to shore, but over a depth of water exceeding the maximum ice thickness. Ice thickness is measured to the nearest centimeter using either a special auger kit or a hot wire ice thickness gauge. Measurements include additional information such as character of ice surface, water features, and method of observations. The comparison of the ice thickness between station measurements and OTIM retrievals were done the same way as that between submarine measurements and OTIM retrievals that is explained in section 4.1.

[34] Figures 6 and 7 show the comparisons of the three data sets, i.e., OTIM using APP-x with station-measured snow depth, PIOMAS simulations, and station measurements at Alert, as a cumulative frequency ice thickness distribution and as point-to-point comparisons. Table 3 gives the statistical results of ice thickness from OTIM and from Canadian stations when both of them have valid ice thickness data and the stations have valid snow depth data. The overall error is comparable to the error of OTIM against submarine data, i.e., 18%. The differences between the OTIM and stations tend to be large when there is ice ridging, rafting, or hummocking at the stations. Besides the error sources discussed in section 4.1, the differences can also be caused by other factors, including point versus area measurements and changing snow conditions over time.

4.3. Comparison With Moored ULS Measurements

[35] The Beaufort Gyre Exploration Project (BGEF) provides ice draft data starting in 2003 from three sites in

Table 2. Geographic Information for the New Arctic Program Stations (Starting Fall 2002) for Ice Thickness and On-Ice Snow Depth Measurements

Station ID	Station Name	Start Date	LAT	LON
LT1	Alert LT1	16 Oct 2002	82.466667	-61.5
YLT	Alert YLT	16 Oct 2002	82.500275	-61.716667
YCB	Cambridge Bay YCB	7 Dec 2002	69.10833	-104.95
YZS	Coral Harbour YZS	15 Nov 2002	64.119446	-82.741669
WEU	Eureka WEU	11 Oct 2002	79.986115	-84.099998
YUX	Hall Beach YUX	10 Nov 2002	68.765274	-80.791664
YEV	Inuvik YEV	29 Nov 2002	68.35833	-132.26138
YFB	Iqaluit YFB	4 Jan 2003	63.727779	-67.48333
YRB	Resolute YRB	13 Dec 2002	74.676941	-93.131668
YZF	Yellowknife YZF	29 Nov 2002	62.465556	-114.36556

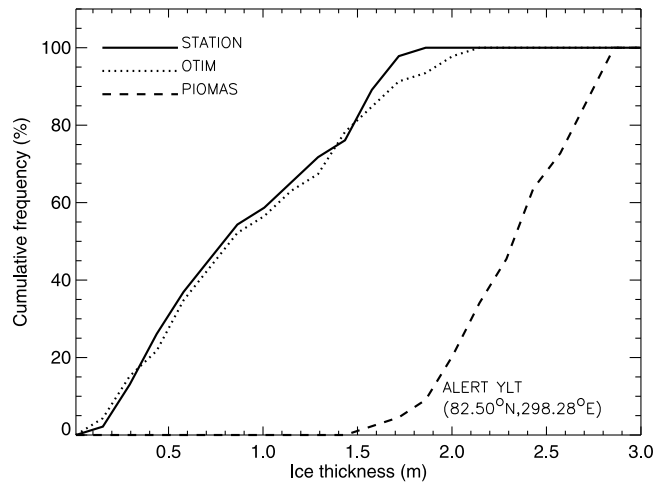


Figure 6. Comparisons of ice thickness cumulative distribution retrieved by OTIM with APP-x data, simulated by PIOMAS model, and measured at Alert.

the Beaufort Sea (<http://www.whoi.edu/beaufortgyre/index.html>). Upward Looking Sonars (ULS) were deployed beneath the Arctic ice pack as part of the Beaufort Gyre Observing System (BGOS; <http://www.whoi.edu/beaufortgyre>) bottom-tethered moorings [Ostrom et al., 2004; Kemp et al., 2005]. Over 15 million observations are acquired for every mooring location in each year. Detailed ULS data processing can be found at http://www.whoi.edu/beaufortgyre/data_moorings_description.html. In this study, ice draft data from 2003 and 2004 at the three mooring sites are used because APP-x data are not available beyond 2004. Daily average ice draft statistics data from the BGOS for 2003 to 2004 were used. The ice draft is converted to ice thickness by a multiplying factor of 1.11, the same process as for submarine ice draft data. Comparison between measurements from moorings and retrievals using OTIM were done the same

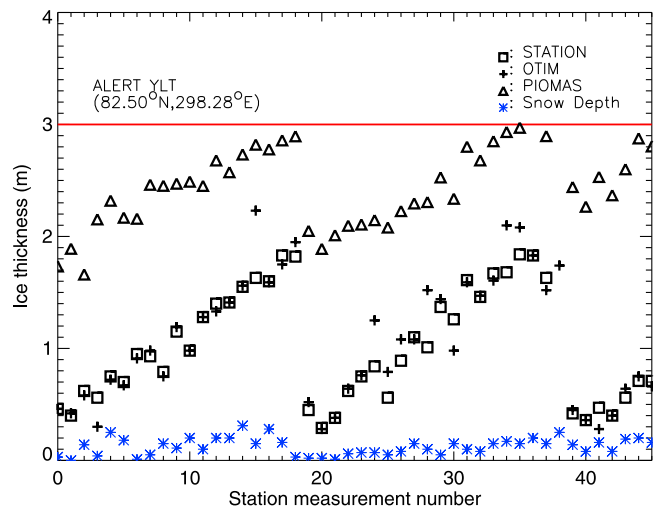


Figure 7. Comparisons of ice thickness values retrieved by OTIM with APPx data and station-measured snow depth data, measured at Alert, and simulated by PIOMAS model.

Table 3. OTIM Retrieved Ice Thickness Validation Results Against Station Measurements From 2002 to 2004^a

Station Name OTIM	Thickness Mean (m)	Bias Mean (m)	Bias Absolute Mean (m)
Alert LT1	1.03	0.05 (4.9%)	0.10 (9.7%)
OTIM	1.08		
Alert YLT	1.03	0.04 (3.9%)	0.10 (9.7%)
OTIM	1.07		
Cambridge Bay YCB	1.32	-0.12 (-9.1%)	0.22 (16.7%)
OTIM	1.20		
Coral Harbour YZS	1.17	-0.19 (-16.2%)	0.20 (17.1%)
OTIM	0.98		
Eureka WEU	1.30	-0.16 (12.3%)	0.22 (16.9%)
OTIM	1.14		
Hall Beach YUX	1.78	-0.13 (-7.3%)	0.32 (18.0%)
OTIM	1.65		
Inuvik YEV	0.95	-0.07 (-7.4%)	0.27 (28.4%)
OTIM	0.88		
Iquluit YFB	1.23	-0.23 (-18.7%)	0.33 (26.8%)
OTIM	1.00		
Resolute YRB	1.35	-0.22 (-16.3%)	0.29 (21.5%)
OTIM	1.13		
Yellowknife YZF	1.15	-0.12 (-10.4%)	0.19 (16.5%)
OTIM	1.03		
All station average	1.23	-0.11 (-8.9%)	0.22 (17.9%)
OTIM average	1.12		

^aThe percentage number in the parentheses is the percent error in terms of true mean ice thickness.

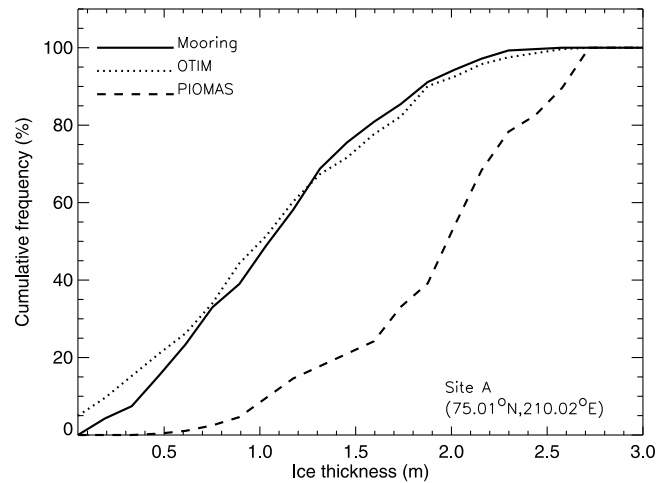
way as that between submarine measurements and retrievals using OTIM.

[36] Table 4 lists mooring site location information, time period, and statistical comparison results. Figures 8 and 9 show the comparisons of the three data sets, i.e., OTIM using APP-x, PIOMAS simulations, and mooring measurements at mooring site A, as a cumulative frequency of ice thickness distribution and as point-to-point comparisons. Table 4 also gives the statistical results of ice thickness from OTIM and from moored ULS measurements for all three sites when both of them have valid ice thickness data. The overall error is comparable to the error of OTIM compared

Table 4. OTIM Retrieved Ice Thickness Validation Results Against Moored ULS Measurements From 2003 to 2004^a

Mooring Location OTIM	Thickness Mean (m)	Bias Mean (m)	Bias Absolute Mean (m)
Site A (75°0.499'N, 149°58.660'W)	1.04	-0.05 (-4.8%)	0.14 (13.5%)
OTIM	0.99		
Site B (78°1.490'N, 149°49.203'W)	1.36	-0.15 (-11.0%)	0.22 (16.2%)
OTIM	1.22		
Site C (76°59.232'N, 139°54.562'W)	1.54	-0.17 (-11.0%)	0.25 (16.2%)
OTIM	1.37		
All mooring average	1.31	-0.12 (-9.2%)	0.20 (15.3%)
OTIM average	1.19		

^aThe percentage number in the brackets is the percent error in terms of true mean ice thickness.

**Figure 8.** Comparisons of ice thickness cumulative distribution retrieved by OTIM with APP-x data, simulated by PIOMAS model, and measured by ULS at the mooring site A.

to station measurements, i.e., 15%. All three comparisons show very similar results with absolute errors less than 20%.

5. Model Uncertainty and Sensitivity

[37] Many factors affect the accuracy of the estimation of ice thickness using the OTIM. Uncertainties in the input variables will ultimately propagate to the ice thickness estimation through the model parameterizations and physics. Theoretically and mathematically, ice thickness is a function of fluxes, surface albedo, and transmittance:

$$\hat{h}_i = f(\hat{\alpha}_s, \hat{i}_0, \hat{F}_r, \hat{F}_l^{up}, \hat{F}_l^{dn}, \hat{F}_s, \hat{F}_e, \hat{F}_c, \hat{F}_a) \quad (11)$$

where variables with carets “^” are the variables defined in equation (1). In the OTIM we use parameterization schemes, as described in previous sections, to calculate \hat{F}_l^{up} , \hat{F}_l^{dn} , \hat{F}_s , \hat{F}_e , \hat{F}_c , all of which are functions of surface skin and air

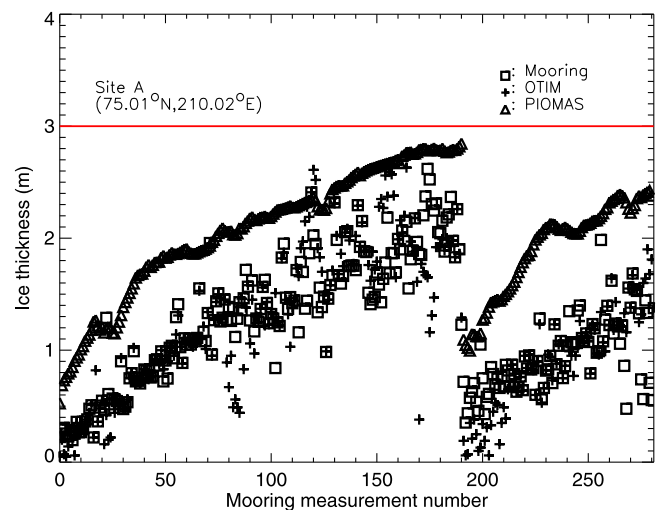
**Figure 9.** Comparisons of ice thickness values retrieved by OTIM with APP-x data, simulated by PIOMAS model, and measured by ULS at the mooring site A.

Table 5. Sensitivity of Ice Thickness Estimation to the Uncertainties in the Controlling Variables for a Daytime Case With Reference Ice Thickness of 1 m^a

Name	Reference Value	Uncertainty (Dx)	IceThk_Dh	IceThk_Dh/Dx
T _s (K)	253.23	+2.000 -2.000	-0.235 +0.245	-0.117 -0.122
T _i (K)	253.23	+5.000 -5.000	-0.008 +0.008	-0.002 -0.002
h _s (m)	0.20	+0.100 -0.100	-0.654 +0.654	-6.544 -6.544
R (%)	90.00	+9.000 -9.000	+0.024 -0.024	+0.003 +0.003
U (m/s)	5.00	+1.000 -1.000	+0.316 -0.208	+0.316 +0.208
P _a (hPa)	1000.00	+50.00 -50.00	+0.066 -0.063	+0.001 +0.001
α _s (0~1)	0.85	+0.100 -0.100	-0.757 +2.195	-7.566 -21.953
T _r (0~1)	0.05	+0.050 -0.050	-0.086 +0.092	-1.711 -1.848
F _r (w/m ²)	101.44	+20.288 -20.288	+0.395 -0.295	+0.019 +0.015
F _a (w/m ²)	0.00	+2.000 -2.000	-0.212 +0.260	-0.106 +0.130
C (0~1)	0.50	+0.250 -0.250	+0.297 -0.639	+1.189 +2.555

^aThe first column lists controlling variable names, the second column contains the reference values of the controlling variables, the third column has the uncertainties of the controlling variables for positive and negative phases, the fourth column gives the errors of the ice thickness estimation resulting from the uncertainties, and the fifth column is the changing rates of ice thickness errors with respect to the controlling variable uncertainties.

temperatures (T_s , T_a), surface air pressure (P_a), surface air relative humidity (R), ice temperature (T_i), wind speed (U), cloud amount (C), and snow depth (h_s). Therefore ice thickness is actually a function of those variables:

$$\hat{h}_i = f(\hat{\alpha}_s, \hat{i}_0, \hat{F}_r, \hat{T}_s, \hat{T}_i, \hat{T}_a, \hat{P}_a, \hat{R}, \hat{U}, \hat{C}, \hat{h}_s, \hat{F}_a) \quad (12)$$

[38] The true ice thickness h_i is estimated from the true values of all the controlling variables in equation (12). Let x_i represent the variables in equation (12) with true values, and let \hat{x}_i represent those variables with estimated values, with x_i subscript i from 1 to 12 representing 12 variables in equation (12). Thus if the uncertainties in the controlling variables are independent and random, error ($\hat{h}_i - h_i$) can be expressed in terms of the uncertainties in the variables on which it depends:

$$(\hat{h}_i - h_i) = \sum (\hat{x}_i - x_i) \frac{\partial h_i}{\partial x_i}, \quad (13)$$

or the variance in the thickness error, as

$$\sigma_{h_i}^2 = \sum \sigma_{x_i}^2 \left(\frac{\partial h_i}{\partial x_i} \right)^2. \quad (14)$$

If, however, as discussed by *Key et al.* [1997b], the variables are not independent, the covariances between them must be considered. Data needed to estimate the covariance between all pairs of variables are often not available. If the covariance between pairs of variables is unknown, it can be shown [Taylor, 1982] that the total uncertainty follow the rule that

$$\sigma_{h_i} \leq \sum \sigma_{x_i} \left| \frac{\partial h_i}{\partial x_i} \right|. \quad (15)$$

[39] Tables 5 and 6 give estimates of the partial derivatives needed in equations (13), (14), and (15), computed using differences ($\Delta h_i / \Delta x_i$). Mathematically, if we know the explicit functional relationship between ice thickness and all its arguments, we could derive partial derivative analytically.

However, ice thickness varies nonlinearly with respect to the parameters under investigation, which are parameterized and/or implicitly involved in the ice thickness calculation, i. e., no explicit functional relationship exists for the analytical partial derivation. Therefore we use numerical method to calculate partial derivatives. These partial derivatives represent the sensitivity of the ice thickness to uncertainties in the controlling variables. The estimated uncertainties in the controlling variables in equation (12), e.g., surface skin temperature T_s , are now used to assess the accuracy of the ice thickness estimation using satellite data products. Since ice thickness varies nonlinearly with respect to the controlling variables, its sensitivity to uncertainties varies over the range of the input controlling variables. Therefore, accuracy in ice thickness is estimated for a reference ice thickness as listed in Tables 5 and 6.

[40] To estimate σ_{h_i} , we need to first estimate the uncertainties of all controlling variables in equation (12). According to *Wang and Key's* [2005] study, for the satellite retrieved surface broadband albedo α_s , the uncertainty would be as large as 0.10 in absolute magnitude. Regarding the ice slab transmittance i_0 , we use an absolute uncertainty of 0.05 in this study, which is probably larger than actual value. Satellite retrieved surface downward shortwave radiation flux F_r can be biased high or low by 20% of the actual value or 35 W m⁻² as compared with in situ measurements [Wang and Key, 2005]. *Wang and Key* [2005] also estimated the uncertainties in satellite-derived surface

Table 6. Same as Table 5 but for a Nighttime Case

Name	Reference Value	Uncertainty (Dx)	IceThk_Dh	IceThk_Dh/Dx
T _s (K)	241.09	+2.000 -2.000	-0.172 +0.179	-0.086 -0.090
T _i (K)	241.09	+5.000 -5.000	-0.008 +0.008	-0.002 -0.002
h _s (m)	0.20	+0.100 -0.100	-0.667 +0.667	-6.666 -6.666
R (%)	90.00	+9.000 -9.000	+0.006 -0.006	+0.001 +0.001
U (m/s)	5.00	+1.0 -1.000	+0.166 -0.133	+0.166 +0.133
P _a (hPa)	1000.00	+50.00 -50.00	+0.043 -0.041	+0.001 +0.001
F _a (w/m ²)	0.00	+2.000 -2.000	-0.137 +0.155	-0.068 +0.078
C (0~1)	0.50	+0.250 -0.250	+0.248 -0.476	+0.992 +1.903

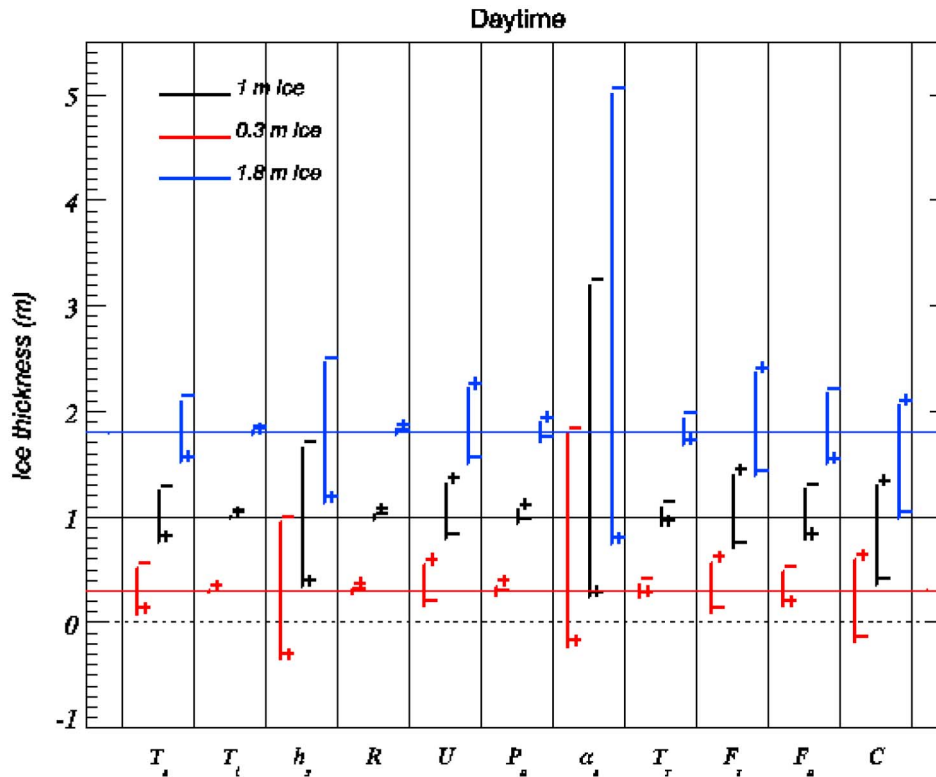


Figure 10. Sensitivity of ice thickness to expected uncertainties in the controlling variables for a daytime case with reference ice thicknesses of 0.3 (red), 1 (black), and 1.8 (blue) m.

skin temperature T_s and cloud amount C with respect to the Surface Heat Balance of the Arctic Ocean (SHEBA) ship measurements [Maslanik *et al.*, 2001], and these uncertainties can be as large as 2 K and 0.25 in absolute magnitude, respectively. We take 2 K as surface air temperature T_a uncertainty. Since the surface may be covered with a layer of snow, the ice slab temperature T_i may be different from T_s . Assuming T_i equal to T_s may introduce additional error in ice thickness estimation. We elect to assign 5 K uncertainty in T_i to estimate its impact on the ice thickness derivation since there is no information about the difference between T_i and T_s , and satellite remote sensing can only retrieve surface skin temperature T_s , not T_i .

[41] The uncertainties in surface air pressure and relative humidity along with surface skin temperature will affect the ice thickness estimation indirectly through the impact of turbulent sensible and latent heat fluxes. A change of 50 hPa surface air pressure may induce changing weather pattern, we take 50 hPa as possible maximum uncertainty of surface air pressure. An uncertainty of 10% in surface air relative humidity is adopted in this work. The uncertainty in geostrophic wind U_G could be 2 m s^{-1} as determined by the buoy pressure field [Thorndike and Colony, 1982], and the relationship $U = 0.34U_G$ gives the uncertainty in surface wind speed U of 0.7 m s^{-1} , we take 1 m s^{-1} as possible actual uncertainty in this study. Snow on the ice directly affects conductive heat flux, surface albedo, and the radiative fluxes at the interface of the ice-snow. Snow depth h_s plays a very important role, but accurate and spatially wide covered measurements are usually not available coincidentally in time and space with satellite observations, and may

change over time with wind and topography. It is difficult to know the uncertainty in snow depth estimation, and we give 50% of the given snow depth as its uncertainty in general. The last uncertainty source is the surface residual heat flux F_a , which is associated with ice melting and possible horizontal heat gain/loss. In the case of no melting and no horizontal heat flux, F_a is zero, which is widely accepted by many sea ice models if the surface temperature is below freezing point. We set uncertainty of F_a 2 W m^{-2} as an initial guess. The overall error in the ice thickness estimation caused by the uncertainties in those controlling variables is less than or equal to the summation of all errors from each individual uncertainty source as mathematically described by equation (15), because the opposite effects may cancel each other.

[42] Tables 5 and 6 list the controlling variables, their uncertainties, and impacts of the uncertainties for daytime and nighttime cases. The results of this sensitivity study are shown graphically in Figures 10 and 11 for the reference ice thickness values of 0.3, 1.0, and 1.8 m with those expected uncertainties in the controlling variables. The bars give the overall ranges in the ice thickness estimation corresponding to the uncertainties listed in the Tables 5 and 6. Plus signs in Figures 10 and 11 are the ice thickness values for positive uncertainties in the indicated variables; minus signs show the changes in ice thickness for negative uncertainties in the controlling variables.

[43] The largest error comes from the surface broadband albedo α_s uncertainty, which can cause more than 200% error in ice thickness estimation. Other error sources are uncertainties in snow depth h_s (65% daytime, 67% night-

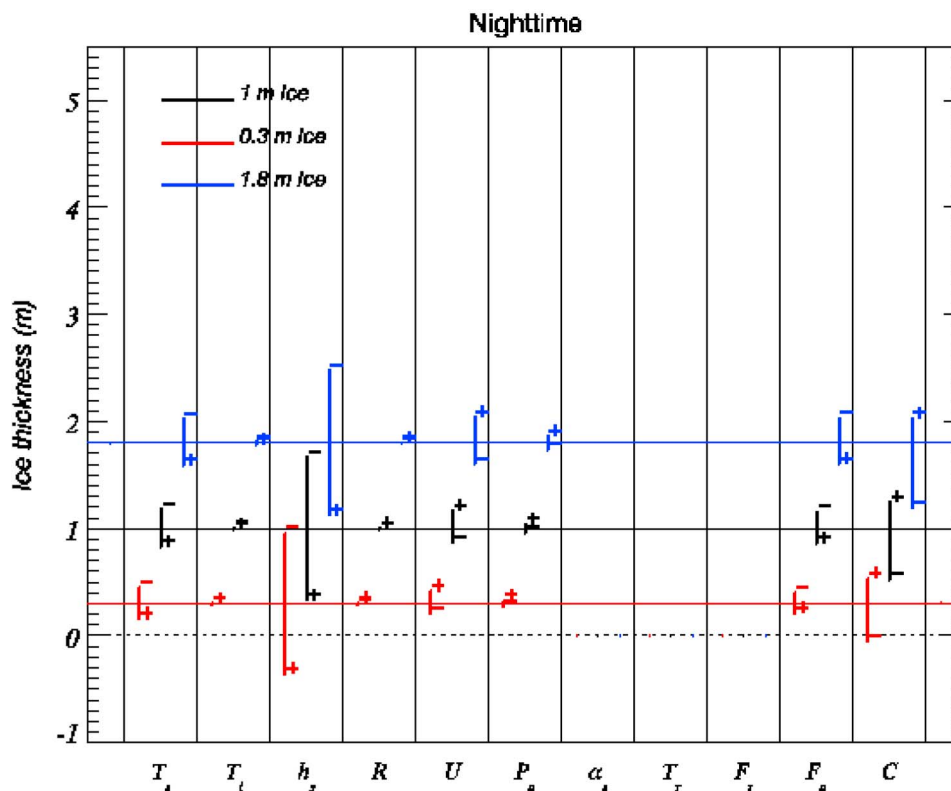


Figure 11. Sensitivity of ice thickness to expected uncertainties in the controlling variables for a nighttime case with reference ice thicknesses of 0.3 (red), 1 (black), and 1.8 (blue) m.

time), cloud amount C (64% daytime, 48% nighttime), surface downward solar radiation flux F_r (40%), surface wind speed U (32% daytime, 17% nighttime), surface residual heat flux F_a (26% daytime, 16% nighttime), surface ice/snow temperature T_s (25% daytime, 18% nighttime), ice slab transmittance T_r (9%), surface air pressure P_a (6.6% daytime, 4.3% nighttime), surface air relative humidity R (2.4% daytime, 0.6% nighttime), and ice temperature T_i (0.8% daytime and nighttime). Obviously, with current retrieval accuracies of surface albedo and shortwave radiation flux from satellite data, it is inappropriate to apply OTIM to daytime data, as doing so may result in very large error in the ice thickness estimation. The sensitivity study also shows a larger error in ice thickness with daytime data than with nighttime data for most of the controlling variables. We thus do not recommend the application of the OTIM to daytime satellite data.

[44] Uncertainties also come from model design structure and parameterization schemes such as the assumed linear vertical temperature profile in the ice slab. Regarding the flux parameterizations that are used in the OTIM, we selected them based on *Key et al.*'s [1996] study on the evaluation of the surface radiative flux parameterization schemes used in different sea ice models. Tables 1–5 in their paper listed errors in the fluxes from different parameterization schemes and their sensitivity to variations in Arctic atmospheric variables such as aerosol, ozone, surface albedo, and clouds. The shortwave and longwave flux parameterization schemes with lower uncertainties have been selected and integrated into OTIM. The evaluation of

the performance of those schemes associated with model structural and parametric selections is beyond the scope of this paper.

6. Conclusions

[45] Due to the uncertainties in the microphysical properties of ice and snow and the uncertainties in satellite-retrieved surface and atmospheric properties, the estimation of ice thickness from space is challenging. Nevertheless, satellite remote sensing offers an unprecedented opportunity to monitor and estimate ice thickness routinely in a large spatial domain with high spatial and temporal resolutions. Here we described a One-dimensional Thermodynamic Ice Model, OTIM, based on the surface energy budget that can instantaneously estimate sea and lake ice thickness with products derived from optical satellite data. This model is not tied to any particular satellite sensor, but instead uses satellite-derived products, generally from visible, near infrared, and infrared imagers, as inputs, e.g., surface skin temperature and cloud cover. Applying this model to AVHRR, MODIS, and SEVIRI products demonstrated that the OTIM performs relatively well with nighttime data, and provides a solid foundation for the use of long-term data from NOAA polar orbiting satellites to generate historical ice thickness records for cryosphere and climate change studies. The model can be used for quantitative estimates of ice thickness up to approximately 2.8 m with an correct accuracy of over 80%.

[46] Validation studies indicate that satellite-derived Arctic sea ice thickness using OTIM has a near-zero mean bias (0.02 m) and a mean absolute bias of 0.18 m when compared to submarine upward looking sonar measurements. The overall bias between ice thickness from the OTIM retrievals and in situ station measurements is -0.11 m, with a mean absolute bias of 0.22 m. Mean bias and mean absolute bias between OTIM retrievals and moored ULS measurements are -0.12 m and 0.20 m, respectively. The estimation error comes from the uncertainties in satellite-derived products, model physics and parameterizations, unknown ice and atmospheric properties, and the inexact collocation of satellite and in situ measurements. It was found that the error tends to be much larger where the ice surface is not smooth, as in the presence of ice ridges, hummocks, or melt ponds. This is not unexpected, as ice dynamics are not included in the OTIM. Comparisons with numerical model simulations demonstrate that the model simulated ice thickness is generally overestimated, especially for relatively thin ice.

[47] In the presence of solar radiation, it is difficult to solve the energy budget equation for ice thickness analytically due to the complex interaction of ice/snow physical properties with solar radiation, which varies considerably with changes in ice/snow clarity, density, chemicals contained, salinity, particle size and shape, and structure. The daytime retrieval is further complicated by inaccuracies in satellite retrievals of surface albedo and the shortwave radiation flux, and the Solar heating on the ice plays significant role in the surface energy budget and makes the residual heat flux not zero due to partial ice melting and horizontal heat flux. We are now working on the parameterization of the surface residual heat flux as a function of atmospheric and surface conditions, i.e., surface albedo, wind, humidity, surface skin and air temperatures, ice thickness, snow depth, cloud amount, and incoming solar radiation flux and/or solar zenith angle, based on station measurements. This way, we will have an OTIM surface energy unbalanced model that will reliably retrieve ice thickness with daytime data. At present, we do not recommend the application of the current OTIM to daytime data.

[48] Applications of the OTIM to satellite data products, in particular, NOAA polar orbiting satellites, will make it possible to routinely monitor rapidly changing sea ice concentration, extent, thickness, and volume, and will provide a better understanding of changes in the cryosphere and climate.

[49] **Acknowledgments.** We would like to thank Jinlun Zhang at the University of Washington for providing PIOMAS simulated Arctic sea ice thickness data and Zhenglong Li at the University of Wisconsin–Madison for helping read out the mooring sea ice draft data in Matlab data format. Thanks also go to the National Snow and Ice Data Center (NSIDC) for providing submarine ice draft data, the Canadian Ice Service (CIS) for providing station-measured Arctic sea ice thickness data, and the Beaufort Gyre Exploration Program based at the Woods Hole Oceanographic Institution (<http://www.whoi.edu/beaufortgyre>) for making mooring data available for us. Finally, we thank the editors and two anonymous reviewers for their helpful comments on the earlier versions of the manuscript. This work was partially supported by the NOAA GOES-R AWG project and the NPOESS Integrated Program Office. The views, opinions, and findings contained in this report are those of the author(s) and should not be construed as an official National Oceanic and Atmospheric Administration or U.S. Government position, policy, or decision.

References

- Ackerman, S. A., K. I. Strabala, W. P. Menzel, R. A. Frey, C. C. Moeller, and L. E. Gumley (1998), Discriminating clear sky from clouds with MODIS, *J. Geophys. Res.*, *103*, 32,141–32,157, doi:10.1029/1998JD200032.
- Andreas, E. L., and S. F. Ackley (1982), On the differences in ablation seasons of Arctic and Antarctic sea ice, *J. Atmos. Sci.*, *39*, 440–447, doi:10.1175/1520-0469(1982)039<0440:OTDIAS>2.0.CO;2.
- Bennett, T. J. (1982), A coupled atmosphere–sea ice model study of the role of sea ice in climatic predictability, *J. Atmos. Sci.*, *39*, 1456–1465, doi:10.1175/1520-0469(1982)039<1456:ACASIM>2.0.CO;2.
- Bentamy, A., K. B. Katsaros, M. Alberto, W. M. Drennan, E. B. Forde, and H. Roquet (2003), Satellite estimates of wind speed and latent heat flux over the global oceans, *J. Clim.*, *16*(4), 637–656, doi:10.1175/1520-0442(2003)016<0637:SEOWSA>2.0.CO;2.
- Berliand, T. C. (1960), Method of climatological estimation of global radiation, *Meteorol. Gidrol.*, *6*, 9–12.
- Cavalieri, D., C. Parkinson, P. Gloersen, and H. J. Zwally (2008), Sea ice concentrations from Nimbus-7 SMMR and DMSP SSM/I passive microwave data, digital media, Natl. Snow and Ice Data Cent., Boulder, Colo.
- Comiso, J. C. (2002), A rapidly declining perennial sea ice cover in the Arctic, *Geophys. Res. Lett.*, *29*(20), 1956, doi:10.1029/2002GL015650.
- Cox, G. F. N., and W. F. Weeks (1974), Salinity variations in sea ice, *J. Glaciol.*, *13*, 109–120.
- Curry, A. J., and P. J. Webster (1999), *Thermodynamics of Atmospheres and Oceans*, 277 pp., Academic, London.
- Doronin, Y. P. (1971), *Thermal Interaction of the Atmosphere and Hydrosphere in the Arctic*, 85 pp., Isr. Program for Sci. Transl, Jerusalem.
- Drobot, S., J. Stroeve, J. Maslanik, W. Emery, C. Fowler, and J. Key (2008), Evolution of the 2007–2008 Arctic sea ice cover and prospects for a new record in 2008, *Geophys. Res. Lett.*, *35*, L19501, doi:10.1029/2008GL035316.
- Ebert, E., and J. A. Curry (1993), An intermediate one-dimensional thermodynamic sea ice model for investigating ice-atmosphere interactions, *J. Geophys. Res.*, *98*, 10,085–10,109, doi:10.1029/93JC00656.
- Efimova, N. A. (1961), On methods of calculating monthly values of net longwave radiation, *Meteorol. Gidrol.*, *10*, 28–33.
- Fowler, C., J. Maslanik, T. Haran, T. Scambos, J. Key, and W. Emery (2007), AVHRR Polar Pathfinder twice-daily 5 km EASE-Grid composites V003, digital media, Natl. Snow and Ice Data Cent., Boulder, Colo.
- Francis, J. A., and E. Hunter (2007), Drivers of declining sea ice in the Arctic winter: A tale of two seas, *Geophys. Res. Lett.*, *34*, L17503, doi:10.1029/2007GL030995.
- Francis, J. A., W. Chan, D. J. Leathers, J. R. Miller, and D. E. Veron (2009), Winter Northern Hemisphere weather patterns remember summer Arctic sea-ice extent, *Geophys. Res. Lett.*, *36*, L07503, doi:10.1029/2009GL037274.
- Grenfell, T. C. (1979), The effects of ice thickness on the exchange of solar radiation over the polar oceans, *J. Glaciol.*, *22*, 305–320.
- Grenfell, T. C., and D. K. Perovich (2004), Seasonal and spatial evolution of albedo in a snow-ice-land-ocean environment, *J. Geophys. Res.*, *109*, C01001, doi:10.1029/2003JC001866.
- Hall, D. K., J. Key, K. A. Casey, G. A. Riggs, and D. J. Cavalieri (2004), Sea ice surface temperature product from the Moderate Resolution Imaging Spectroradiometer (MODIS), *IEEE Trans. Geosci. Remote Sens.*, *42*(5), 1076–1087, doi:10.1109/TGRS.2004.825587.
- Jacobs, J. D. (1978), Radiation climate of Broughton Island, in *Energy Budget Studies in Relation to Fast-Ice Breakup Processes in Davis Strait*, edited by R. G. Barry and J. D. Jacobs, *Occas. Pap.* 26, pp. 105–120, Inst. of Arctic and Alp. Res., Univ. of Colo., Boulder.
- Jin, Z., K. Stamnes, and W. F. Weeks (1994), The effect of sea ice on the solar energy budget in the atmosphere–sea ice–ocean system: A model study, *J. Geophys. Res.*, *99*(C12), 25,281–25,294, doi:10.1029/94JC02426.
- Kara, A. B., P. A. Rochford, and H. E. Hurlburt (2000), Efficient and accurate bulk parameterizations of air–sea fluxes for use in general circulation models, *J. Atmos. Oceanic Technol.*, *17*, 1421–1438.
- Kemp, J., K. Newhall, W. Ostrom, R. Krishfield, and A. Proshutinsky (2005), The Beaufort Gyre Observing System 2004: Mooring recovery and deployment operations in pack ice, *Tech. Rep. Woods Hole Oceanogr. Inst. WHOI-2005-05*, 33 pp., Woods Hole, Mass., doi:10.1575/1912/73.
- Key, J. (2002), *The Cloud and Surface Parameter Retrieval (CASPR)*, 62 pp., System for Polar AVHRR Data User’s Guide, Space Science and Engineering Center, Univ. of Wisc., Madison.
- Key, J. R., R. A. Silcox, and R. S. Stone (1996), Evaluation of surface radiative flux parameterizations for use in sea ice models, *J. Geophys. Res.*, *101*(C2), 3839–3849, doi:10.1029/95JC03600.

- Key, J., J. Collins, C. Fowler, and R. Stone (1997a), High-latitude surface temperature estimates from thermal satellite data, *Remote Sens. Environ.*, *61*, 302–309, doi:10.1016/S0034-4257(97)89497-7.
- Key, J., A. J. Schweiger, and R. S. Stone (1997b), Expected uncertainty in satellite-derived estimates of the surface radiation budget at high latitudes, *J. Geophys. Res.*, *102*(C7), 15,837–15,847, doi:10.1029/97JC00478.
- Kovacs, A. (1996), Sea ice: Part I. Bulk salinity versus ice floe thickness, *CRREL Rep. 96-7*, U.S. Army Cold Reg. Res. and Eng. Lab., Hanover, N. H.
- Kwok, R., and G. F. Cunningham (2008), ICESat over Arctic sea ice: Estimation of snow depth and ice thickness, *J. Geophys. Res.*, *113*, C08010, doi:10.1029/2008JC004753.
- Kwok, R., G. F. Cunningham, M. Wensnahan, I. Rigor, H. J. Zwally, and D. Yi (2009), Thinning and volume loss of the Arctic Ocean sea ice cover: 2003–2008, *J. Geophys. Res.*, *114*, C07005, doi:10.1029/2009JC005312.
- Laevastu, T. (1960), Factors affecting the temperature of the surface layer of the sea, *Comments Phys. Math.*, *25*(1), 136 pp.
- Laxon, S., N. Peacock, and D. Smith (2003), High interannual variability of sea ice thickness in the Arctic region, *Nature*, *425*, 947–950, doi:10.1038/nature02050.
- Lindsay, R. W. (1998), Temporal variability of the energy balance of thick Arctic pack ice, *J. Clim.*, *11*, 313–333, doi:10.1175/1520-0442(1998)011<0313:TVOTEB>2.0.CO;2.
- Liu, Y. H., J. R. Key, R. A. Frey, S. A. Ackerman, and W. P. Menzel (2004), Nighttime polar cloud detection with MODIS, *Remote Sens. Environ.*, *92*, 181–194, doi:10.1016/j.rse.2004.06.004.
- Maslanik, J. A., J. Key, C. W. Fowler, T. Nguyen, and X. Wang (2001), Spatial and temporal variability of satellite-derived cloud and surface characteristics during FIRE-ACE, *J. Geophys. Res.*, *106*(D14), 15,233–15,249, doi:10.1029/2000JD900284.
- Maslanik, J. A., C. Fowler, J. Stroeve, S. Drobot, J. Zwally, D. Yi, and W. Emery (2007), A younger, thinner Arctic ice cover: Increased potential for rapid extensive sea-ice loss, *Geophys. Res. Lett.*, *34*, L24501, doi:10.1029/2007GL032043.
- Maykut, G. A., and P. E. Church (1973), Radiation climate of Barrow, Alaska, 1962–66, *J. Appl. Meteorol.*, *12*, 620–628, doi:10.1175/1520-0450(1973)012<0620:RCOBA>2.0.CO;2.
- Maykut, G. A., and N. Untersteiner (1971), Some results from a time-dependent thermodynamic model of sea ice, *J. Geophys. Res.*, *76*, 1550–1575, doi:10.1029/JC076i006p01550.
- Moritz, R. E. (1978), A model for estimating global solar radiation, in *Energy Budget Studies in Relation to Fast-Ice Breakup Processes in Davis Strait*, edited by R. G. Barry and J. D. Jacobs, *Occas. Pap. 26*, pp. 121–142, Inst. of Arctic and Alp. Res., Univ. of Colo., Boulder.
- National Snow and Ice Data Center (2006), Submarine upward looking sonar ice draft profile data and statistics, digital media, World Data Cent. for Glaciol., Boulder, Colo.
- Ohmura, A. (1981), Climate and energy balance of the Arctic tundra, *Zürcher Geogr. Schr.* *3*, 448 pp., Geogr. Inst., Zurich, Switzerland.
- Ostrom, W., J. Kemp, R. Krishfield, and A. Proshutinsky (2004), Beaufort Gyre Freshwater Experiment: Deployment Operations and Technology in 2003, *Tech. Rep. Woods Hole Oceanogr. Inst. WHOI-2004-01*, 32 pp., Woods Hole, Mass.
- Persson, P. O. G., C. W. Fairall, E. L. Andreas, P. S. Guest, and D. K. Perovich (2002), Measurements near the Atmospheric Surface Flux Group tower at SHEBA: Near-surface conditions and surface energy budget, *J. Geophys. Res.*, *107*(C10), 8045, doi:10.1029/2000JC000705.
- Rees, W. G. (1993), Infrared emissivities of Arctic land cover types, *Int. J. Remote Sens.*, *14*, 1013–1017, doi:10.1080/01431169308904392.
- Rothrock, D., D. B. Percival, and M. Wensnahan (2008), The decline in arctic sea-ice thickness: Separating the spatial, annual, and interannual variability in a quarter century of submarine data, *J. Geophys. Res.*, *113*, C05003, doi:10.1029/2007JC004252.
- Saloranta, T. M. (2000), Modeling the evolution of snow, snow ice and ice in the Baltic Sea, *Tellus, Ser. A*, *52*, 93–108.
- Schmetz, P. J., and E. Raschke (1986), Estimation of daytime downward longwave radiation at the surface from satellite and grid point data, *Theor. Appl. Climatol.*, *37*, 136–149, doi:10.1007/BF00867847.
- Shine, K. P. (1984), Parameterization of shortwave flux over high albedo surfaces as a function of cloud thickness and surface albedo, *Q. J. R. Meteorol. Soc.*, *110*, 747–764, doi:10.1002/qj.49711046511.
- Shine, K. P., and A. Henderson-Sellers (1985), The sensitivity of a thermodynamic sea ice model to changes in surface albedo parameterization, *J. Geophys. Res.*, *90*, 2243–2250, doi:10.1029/JD090iD01p02243.
- Taylor, J. R. (1982), *An Introduction to Error Analysis*, 270 pp., Univ. Sci. Books, Mill Valley, Calif.
- Thorndike, A. S., and R. Colony (1982), Sea ice motion in response to geostrophic winds, *J. Geophys. Res.*, *87*(C8), 5845–5852, doi:10.1029/JC087iC08p05845.
- Untersteiner, N. (1964), Calculations of temperature regime and heat budget of sea ice in the central Arctic, *J. Geophys. Res.*, *69*, 4755–4766, doi:10.1029/JZ069i022p04755.
- Wang, X., and J. Key (2003), Recent trends in Arctic surface, cloud, and radiation properties from space, *Science*, *299*(5613), 1725–1728, doi:10.1126/science.1078065.
- Wang, X., and J. Key (2005), Arctic surface, cloud, and radiation properties based on the AVHRR Polar Pathfinder data set. Part I: Spatial and temporal characteristics, *J. Clim.*, *18*(14), 2558–2574, doi:10.1175/JCLI3438.1.
- Wang, X., J. R. Key, C. Fowler, and J. Maslanik (2007), Diurnal cycles in Arctic surface radiative fluxes in a blended satellite–climate reanalysis data set: Algorithm description, validations, and preliminary results, *J. Appl. Remote Sens.*, *1*, 013535, doi:10.1117/1.2794003.
- Yen, Y.-C. (1981), Review of thermal properties of snow, ice and sea ice, *CRREL Rep. 81-10*, 27 pp., Cold Reg. Res. and Eng. Lab., Hanover, N. H.
- Yu, Y., and D. A. Rothrock (1996), Thin ice thickness from satellite thermal imagery, *J. Geophys. Res.*, *101*(C11), 25,753–25,766, doi:10.1029/96JC02242.
- Zhang, J., and D. A. Rothrock (2001), A thickness and enthalpy distribution sea-ice model, *J. Phys. Oceanogr.*, *31*, 2986–3001, doi:10.1175/1520-0485(2001)031<2986:ATAEDS>2.0.CO;2.
- Zhang, J., and D. A. Rothrock (2003), Modeling global sea ice with a thickness and enthalpy distribution model in generalized curvilinear coordinates, *Mon. Weather Rev.*, *131*(5), 845–861, doi:10.1175/1520-0493(2003)131<0845:MGSIIWA>2.0.CO;2.
- Zhang, X., and J. E. Walsh (2006), Toward seasonally ice-covered Arctic Ocean: Scenarios from the IPCC AR4 model simulations, *J. Clim.*, *19*, 1730–1747, doi:10.1175/JCLI3767.1.
- Zillman, J. W. (1972), A study of some aspects of the radiation and heat budgets of the southern hemisphere oceans, *Meteorol. Stud. Rep. 26*, Bur. of Meteorol., Dep. of the Inter., Canberra.
- Zwally, H. J., D. Yi, R. Kwok, and Y. Zhao (2008), ICESat measurements of sea ice freeboard and estimates of sea ice thickness in the Weddell Sea, *J. Geophys. Res.*, *113*, C02S15, doi:10.1029/2007JC004284.

J. R. Key, NESDIS, NOAA, 1225 W. Dayton St., Madison, WI 53706, USA.

Y. Liu and X. Wang, Cooperative Institute of Meteorological Satellite Studies, University of Wisconsin–Madison, 1225 W. Dayton St., Madison, WI 53706, USA. (xuanjiw@ssec.wisc.edu)